ISSN 0018-151X, High Temperature, 2011, Vol. 49, No. 5, pp. 704–711. © Pleiades Publishing, Ltd., 2011.
Original Russian Text © D.Yu. Adamian, A.K. Travin, 2011, published in Teplofizika Vysokikh Temperatur, 2011, Vol. 49, No. 5, pp. 728–736.

HEAT AND MASS TRANSFER AND PHYSICAL GASDYNAMICS

Improved Version of the Synthetic Eddy Method for Setting Nonstationary Inflow Boundary Conditions in Calculating Turbulent Flows

D. Yu. Adamian and A. K. Travin

St. Petersburg State Polytechnical University, ul. Politekhnicheskaya 29, St. Petersburg, 195251 Russia

e-mail: d_adamian@mail.ru

Received February 17, 2010

Abstract—One method for generating synthetic turbulence, i.e., the synthetic eddy method, is tested by means of the example of canonical turbulent shear flows (plane-channel and boundary-layer flows). A modification of the method, differing from the original version by the determination of the linear scale of synthetic eddy structures, is proposed. The synthetic field of turbulent fluctuations evolves more quickly to the physically realistic one when the modified method is used instead of the original one. The friction coefficient and profiles of the average velocity and Reynolds stresses also deviate less and recover faster if the modified method is used.

DOI: 10.1134/S0018151X11040018

INTRODUCTION

One of the principal problems associated with calculation of turbulent flows using large eddy simulation (LES) method is the necessity of setting unsteady boundary conditions at the inflow boundaries of the calculation region that will extremely accurately correspond to the actual characteristics of turbulence at these boundaries. Recently, this problem became especially acute in connection with the active development of the so-called zone approaches to the turbulence description, based on the use of the LES only in a limited flow region and the description of the other region within the Reynolds averaged Navier–Stokes (RANS) equations [1]. In this case, realistic turbulent characteristics of the flow should be set at outflow boundaries of the RANS region, which are simultaneously inflow boundaries of the LES region. Unfortunately, an ideal solution of this problem is essentially impossible, and the case in point can be only more or less efficient approximate approaches, to whose development a large number of studies is devoted. As a result, a rather wide spectrum of methods were proposed (see, e.g., review [2]), which can be divided into three main groups.

In the first-group methods, the boundary conditions for LES inflow boundaries are set using properly scaled results of direct numerical simulation (DNS), known for some certain "canonical" turbulent flows, e.g., for the developed channel and flat-plate boundary-layer flows at low Reynolds numbers. These methods are accurate; however, their applicability is restricted to a narrow class of flows rather close to canonical ones.

Methods that are conventionally referred to as turbulence "recycling" belong to the second group. Within these methods, the turbulent flow characteristics at the LES inflow boundary are calculated by their transfer from a certain section within the LES region. In this case, changes in turbulence characteristics in the interval from the inflow boundary to the recycling section are taken into account based on available theoretical concepts on the evolution of averaged parameters of the downstream flow. In principle, recycling methods yield quite realistic parameters of turbulent pulsations at the inflow boundary of the LES region and, in contrast to the first-group methods, are closed (do not require any external information). However, their applicability region is very limited, since the laws of evolution of averaged parameters of turbulent downstream flows are known only for relatively simple cases. Furthermore, when using the recycling methods, a false resonant peak which appears in the turbulence spectrum, whose frequency is related to the distance from the inflow section to the recycling section (this disadvantage is of particular importance for aeroacoustic applications).

Finally, the third group of methods is based on setting an artificial ("synthetic") turbulence in the inflow section of the LES region; i.e., nonstationary velocity pulsations that correspond to one extent or another to actual turbulence in the section under consideration. Generally speaking, these methods are more versatile and universal than the methods of the first two groups; however, their accuracy depends heavily on a particular method of synthetic turbulence generation. Analysis of publications devoted to this problem evidences that one of the most efficient (economic and accurate) methods is the synthetic eddy method (SEM) proposed in [2, 3]. In particular, the SEM makes it possible to appreciably shorten the length of the intermediate region inevitably arising during the transition from the synthetic to actual turbulence, which noticeably improves the calculation accuracy in comparison with other known methods of synthetic turbulence generation, e.g., the method of [4]. Nevertheless, when using the SEM, this region remains rather extended (its length is on the order of (8–10)δ, where δ is the characteristic thickness of the boundary layer).

In this paper, based on an analysis of the results calculated using the SEM, an advanced version of this method is proposed, which allows significant shortening of the intermediate region.

The structure of the paper is as follows.

In Section 1, basic equations of the LES method for a viscous incompressible liquid are formulated and a numerical method used for calculations are presented. In Section 2, the SEM is briefly described; in Section 3, the LES results obtained using this method in calculating the developed turbulent plane-channel and turbulent flat-plate boundary-layer flows are described and analyzed. Finally, Section 4 presents the proposed SEM modification and the results of the solution of the same problems obtained using the SEM. In the Conclusions, the main results of the study are briefly formulated.

1. LES MEHOD EQUATIONS AND NUMERICAL METHOD USED FOR THEIR SOLUTION

Spatially filtered Navier–Stokes equations for an incompressible liquid in combination with the linear subgrid model of eddy viscosity can be written in the form

$$\nabla \cdot \mathbf{V} = 0,$$

$$\partial \mathbf{V}/dt + (\mathbf{V}\nabla)\mathbf{V} = -\frac{1}{\rho}\nabla p + \nabla \cdot ((\nu + \nu_{\mathrm{SGS}})\nabla \mathbf{V}),$$

where $\mathbf{V}$ and p are the filtered velocity vector and pressure; ρ is the constant liquid density; and ν and ν_{SGS} are the coefficients of molecular and subgrid kinematic viscosity, respectively. The latter is defined using the simplest Smagorinsky algebraic model with the Van Driest damping factor [5],

$$\nu_{\mathrm{SGS}} = \min((\kappa y)^2, (C_{\mathrm{Smag}}\Delta)^2)[1 - \exp(-(y^+/25)^3)]S. \tag{1}$$

where $S = \sqrt{2S_{ij}S_{ij}}$, S_{ij} are components of the strain rate tensor, $y^+ = y\sqrt{\tau_w/\rho}/\nu$ is the universal coordinate of the wall law (τ_w is the friction stress on the wall), Δ is the subgrid linear scale, $\kappa = 0.41$ is the Karman constant, and C_{Smag} is the Smagorinsky empirical constant.

The subgrid linear scale entering Eq. (1) was defined according to [6],

$$\Delta = \min(\max(C_w d_w, C_w h_{\max}, h_{wn}), h_{\max}),$$

where d_w is the distance from the point under consideration to the streamlined solid surface, $h_{\max} = \max(h_x, h_y, h_z)$ maximum grid spacing, h_{wn} is the grid spacing along the normal to the streamlined surface, and $C_w = 0.15$ is the empirical constant.

As shown in [6], such a definition of the subgrid scale Δ makes it possible to describe near-wall and free turbulent flows using the same Smagorinsky constant in (1). In this study, this value was set equal to 0.2 (it provides an accurate slope of the spectrum of decaying homogeneous isotropic turbulence in the inertial range of wavenumbers).

All calculations presented below are performed using the NTS code described in [7]. To calculate incompressible liquid flows, the method of [8] is used. In this case, to approximate nonviscous and viscous flows, the symmetric fourth-order-accuracy finite volume and symmetric second-order approximations, respectively, were used in basic equations. Time integration is performed using the implicit second-order-accuracy three-layer scheme with internal pseudotime iterations. To solve systems of linear equations obtained by discretizing basic differential equations, the diagonally?dominant alternating direction implicit (DDADI) is used.

2. SYNTHETIC EDDY METHOD

A detailed description and validation of the SEM are contained in [2]; therefore, here we present only details of implementation of the method.

Let the inflow boundary of the LES region on which hydrodynamic value fluctuations ("synthetic eddies") should be created be a surface S given by a set of points $\mathbf{x} = \{\mathbf{x}_1, \mathbf{x}_2, \ldots, \mathbf{x}_s\}$; the parallelepiped B with volume V_B incorporates this surface. The minimum and maximum coordinates of parallelepiped points are defined as $x_{i,\min} = \min\limits_{\mathbf{x} \in S}[x_i - \sigma(\mathbf{x})]$ and $x_{i,\max} = \max\limits_{\mathbf{x} \in S}[x_i + \sigma(\mathbf{x})]$, where σ is the linear scale of synthetic fluctuations, which defined below. Then the velocity vector components at the inflow boundary are calculated as

$$u_i(\mathbf{x}) = U_i(\mathbf{x}) + \frac{1}{N}\sum_{k=1}^{N} a_{ij}\varepsilon_j^k f_\sigma(\mathbf{x} - \mathbf{x}^k). \tag{2}$$

Here U_i are the components of the averaged flow velocity at points of the inflow section, which are assumed to be known, and $N = \max(V_B/\sigma^3)$ is the number of generated synthetic eddies; the arrangement $\mathbf{x}^k$ and components ε_j^k of the intensity vector of individual "eddies" are independent random variables equiprobably taking the values of +1 and –1.

The function $f_\sigma(\mathbf{x}-\mathbf{x}^k)$ in (2), defining the velocity distribution in the eddy is given by

$$f_\sigma(\mathbf{x}-\mathbf{x}^k) = \sqrt{V_B}\sigma^{-3}\prod_{i=1}^{3} f((x_i - x_i^k)/\sigma),$$

where the one-dimensional distribution function f is calculated by the formula

$$f(x) = \begin{cases} (3/2)^{1/2}(1-|x|) & \text{at } |x| < 1, \\ 0 & \text{at } |x| \geq 1. \end{cases}$$

The quantity a_{ij} entering (2) means components of the Cholesky decomposition of the Reynolds stress tensor (as a result of its introduction, the Reynolds stresses calculated by velocity fluctuations defined by relation (4) coincide with their specified distributions).

Finally, the linear scale σ defining synthetic eddy sizes is calculated by the formula

$$\sigma = \max(\min(l_{\text{turb}}, \kappa\delta), \Delta). \tag{3}$$

Here $\Delta = \max(\Delta x, \Delta y, \Delta z)$ is the maximum grid spacing, l_{turb} is the integral turbulence scale in the LES inflow section, and δ is the characteristic flow macroscale (e.g., the boundary layer thickness).

In this study, the average velocity in the inflow section is determined within the RANS using the Menter k–ω SST model [9], in which the integral scale is $l_{\text{turb}} = k_t^{3/2}/C_\mu\omega_t$ k_t is the kinetic energy of turbulence, ω_t is the specific velocity of its dissipation, and $C_\mu = 0.09$).

The time dependence of velocity field (2) is set as follows. It is assumed that eddies are transferred within the parallelepiped B with constant velocity $\mathbf{U_c}$ equal to the average flow velocity in the inflow section. Thus, for one time step Δt, the kth eddy moves to distance $\mathbf{U_c}\Delta t$: $\mathbf{x}^k(t+\Delta t) = \mathbf{x}^k(t) + \mathbf{U_c}\Delta t$. If it appears beyond the parallelepiped B boundary through the boundary F during the calculation, an eddy with a new random intensity vector $\varepsilon_j^k = \pm 1.$ is placed at a random point of the opposite parallelepiped boundary. At the first time step, points $\mathbf{x}^k$ are randomly uniformly distributed within parallelepiped B.

Thus, the SEM creates a stochastic velocity field with given average velocity components U_i, Reynolds stresses, and linear scales σ on the surface S.

3. RESULTS CALCULATED USING THE SEM AND THEIR ANALYSIS

To estimate the accuracy of the unsteady boundary conditions created by the SEM, LES calculations of the developed plane-channel and flat-plate boundary-layer flows were performed using this method. In this case, the results obtained using periodic boundary conditions along the longitudinal coordinate and the results of calculations by the turbulence recycling method [10, 11] (as shown in these papers, this method provides rather high calculation accuracy in this case) were used as "references" for the first and second problems, respectively.

3.1. Statement of the Problem of the Steady Turbulent Plane-Channel Flow

This flow was calculated for the Reynolds number constructed by the dynamic velocity $\sqrt{\tau_w/\rho}$, channel half-width δ and viscosity ν, and $\text{Re}_\tau = 400$ (the Reynolds number constructed by the average-rate velocity U_b is 7×10^3). The computational domain dimension was $8\delta \times 2\delta \times 3\delta$ in x, y, and z directions (along the flow, along the normal to channel walls, and across the flow), respectively.

In reference calculations, adhesion boundary conditions $\mathbf{V} = 0$ on channel walls were set; periodicity conditions were applied to boundaries along longitudinal and transverse coordinates. In the calculations, the same boundary conditions were used for walls and transverse boundaries of the region; conditions at the inflow boundary were set using relations (2) and (3). In this case, the average velocity profiles and turbulent characteristics k_t and ω_t were determined from the preliminary RANS calculation using the k–ω SST model [9]. A constant pressure was set at the outflow boundary of the computational domain.

Both calculations were performed on the same grid uniform along x and z and a nonuniform (densifying in the channel wall direction) grid with dimensions of $81 \times 84 \times 41$ (278964 nodes). The spacings of his grid in the units of the wall rule are $\Delta x^+ = 40$, $\Delta z^+ = 20$, $\Delta y^+_{\min} = 0.9$ and $\Delta y^+_{\max} = 23$, which a priori satisfies the requirements imposed on grids for LES near-wall flows.

3.2. Statement of the Problem of Turbulent Flat-Plate Boundary-Layer Flow

This flow was calculated in the variation range of the Reynolds numbers constructed by the momentum loss thickness, $\text{Re}_\theta = 1200$–1700. The computational domain size was $20\delta_0 \times 4\delta_0 \times 3\delta_0$ (δ_0 is the boundary layer thickness in the inflow section) in the x, y, and z directions, respectively. On the plate surface ($y = 0$), the adhesion conditions $\mathbf{V} = 0$ were used; at the region boundaries along the z coordinate, periodicity conditions were set; and, at the outflow boundary, the pressure constancy condition was set.

To set the conditions at the inflow boundary, the "recycling" method was used in reference calculations [11]; in SEM calculations, the synthetic velocity field constructed by the average velocity profiles and turbu-

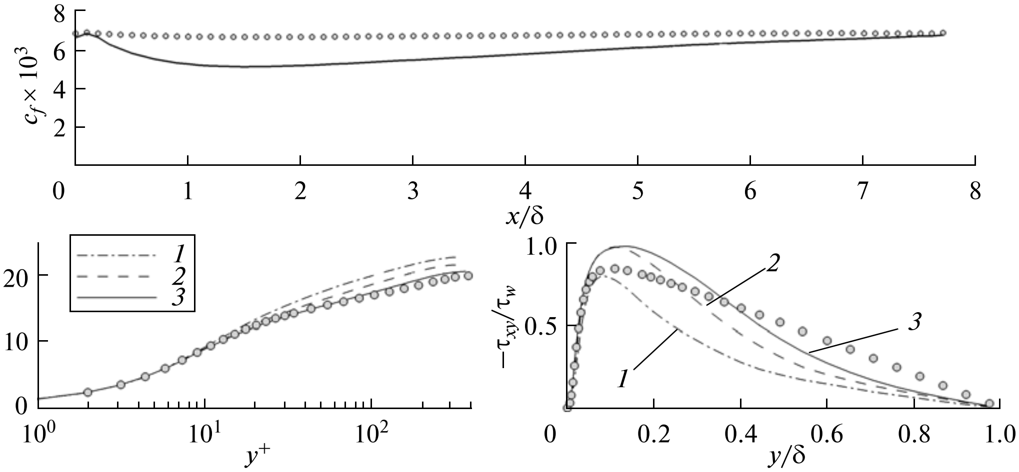

Fig. 1. Comparison of the distributions of the friction coefficient c_f, average velocity profiles, and Reynolds shear stress profiles in the various sections of the plane-channel flow, obtained in "reference" calculations (circles) and SEM calculations (curves) for sections x/δ_0 = (curve *1*) 2, (curve *2*) 4, and (curve *3*) 6.

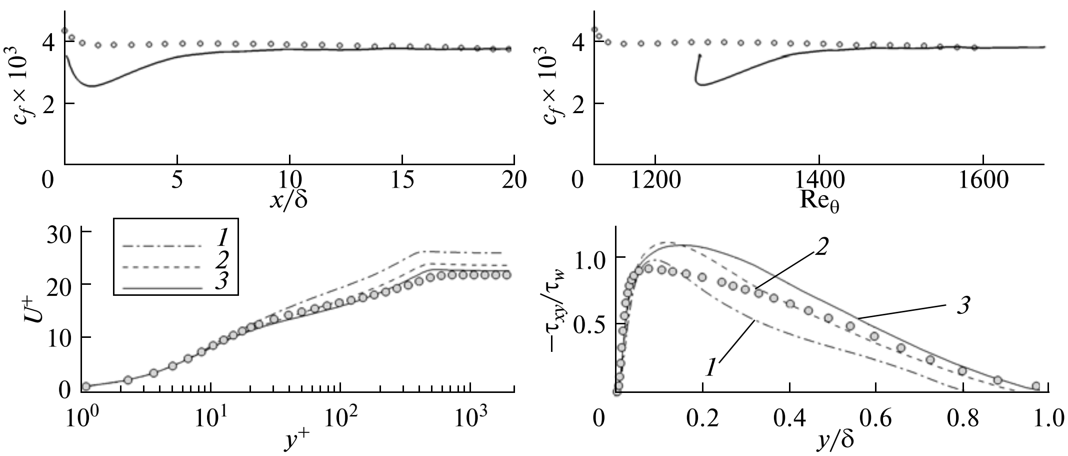

Fig. 2. Comparison of the distributions of the friction coefficient c_f, average velocity profiles, and Reynolds shear stress profiles in the various sections of the boundary-layer flow, obtained in "reference" calculations (circles) and SEM calculations (curves) for sections x/δ_0 = (curve *1*) 2, (curve *2*) 4, and (curve *3*) 6.

lence characteristics obtained from the preliminary RANS calculation was used.

As in the case of the plane channel, both calculations were performed on the same grid with dimension $257 \times 56 \times 78$ (only 1 122 576 nodes) with densification along the normal to the plate in a geometrical progression with an exponent of 1.1. In the units of the wall law, the grid spacing is close to that of the grid used in the calculation of the plane-channel flow, $\Delta x^+ \approx 40$, $\Delta z^+ \approx 20$, $\Delta y^+_{\min} \approx 1.0$, and $\Delta y^+_{\max} \approx 180$.

3.3. Calculation Results

Figures 1 and 2 compare the longitudinal distributions of the friction coefficient c_f and the profiles of the average velocity and Reynolds shear stresses in various flow sections, obtained from reference calculations of plane-channel and boundary-layer flows and from similar SEM calculations.

We can see that, when using the SEM, the friction coefficient in both cases initially significantly deviates from the reference distribution and then gradually approaches it. For the channel flow, the maximum deviation is observed at distance (1–2)δ from the inflow section and its value is 20–25%. The friction coefficient is almost completely restored in the section $x = 8\delta$. For the boundary-layer flow, the c_f distribution deviation on the plate from the reference one reaches 30–35% and decreases to 5% only in the section $x = 10\delta$.

The same trends are observed in the behavior of average velocity profiles (see Figs. 1 and 2): near the initial section, they differ significantly from the reference

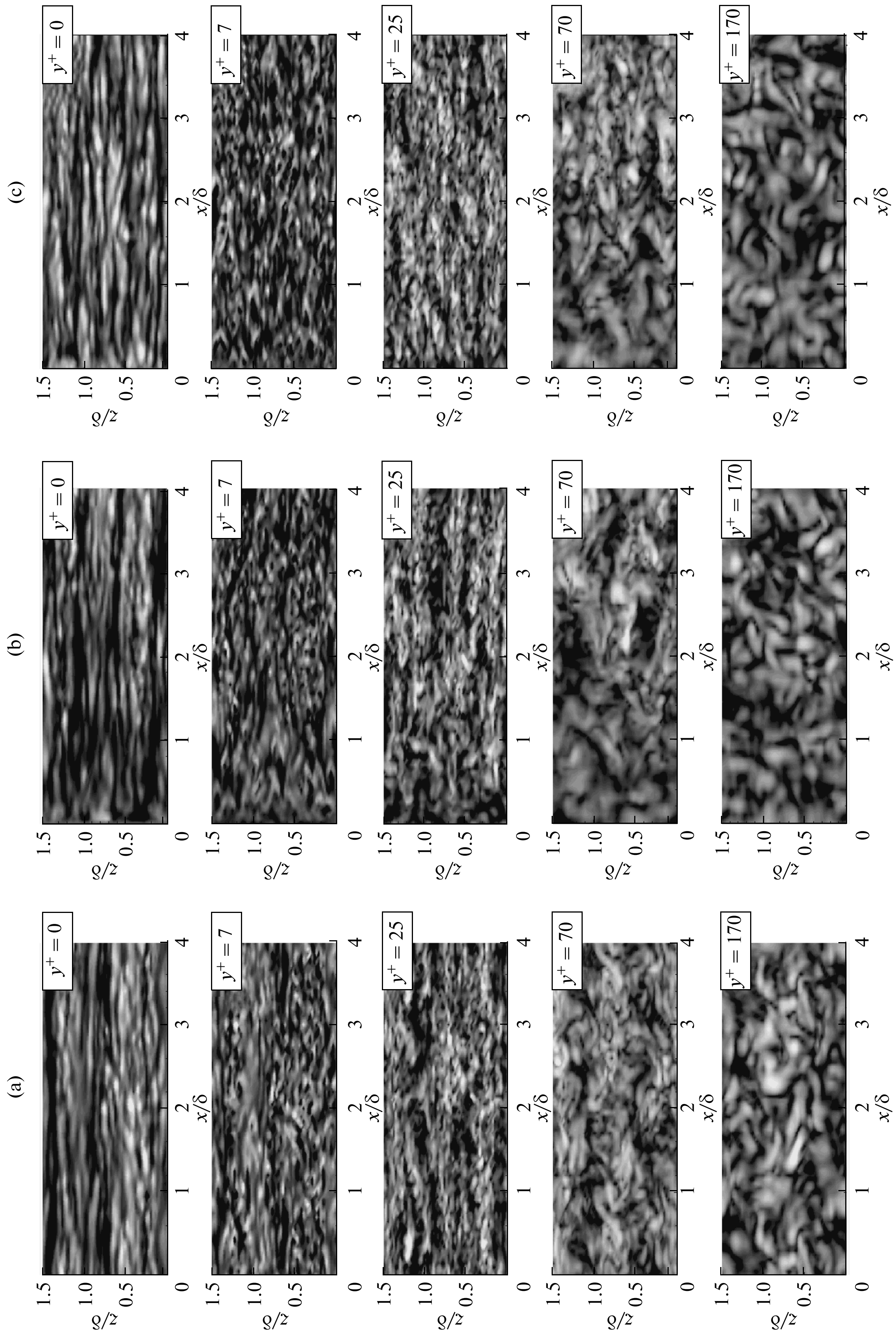

Fig. 3. Comparison of the instantaneous eddy fields in planes x–z for (a) the "reference" calculation and calculations using the (b) initial and (c) modified SEM methods.

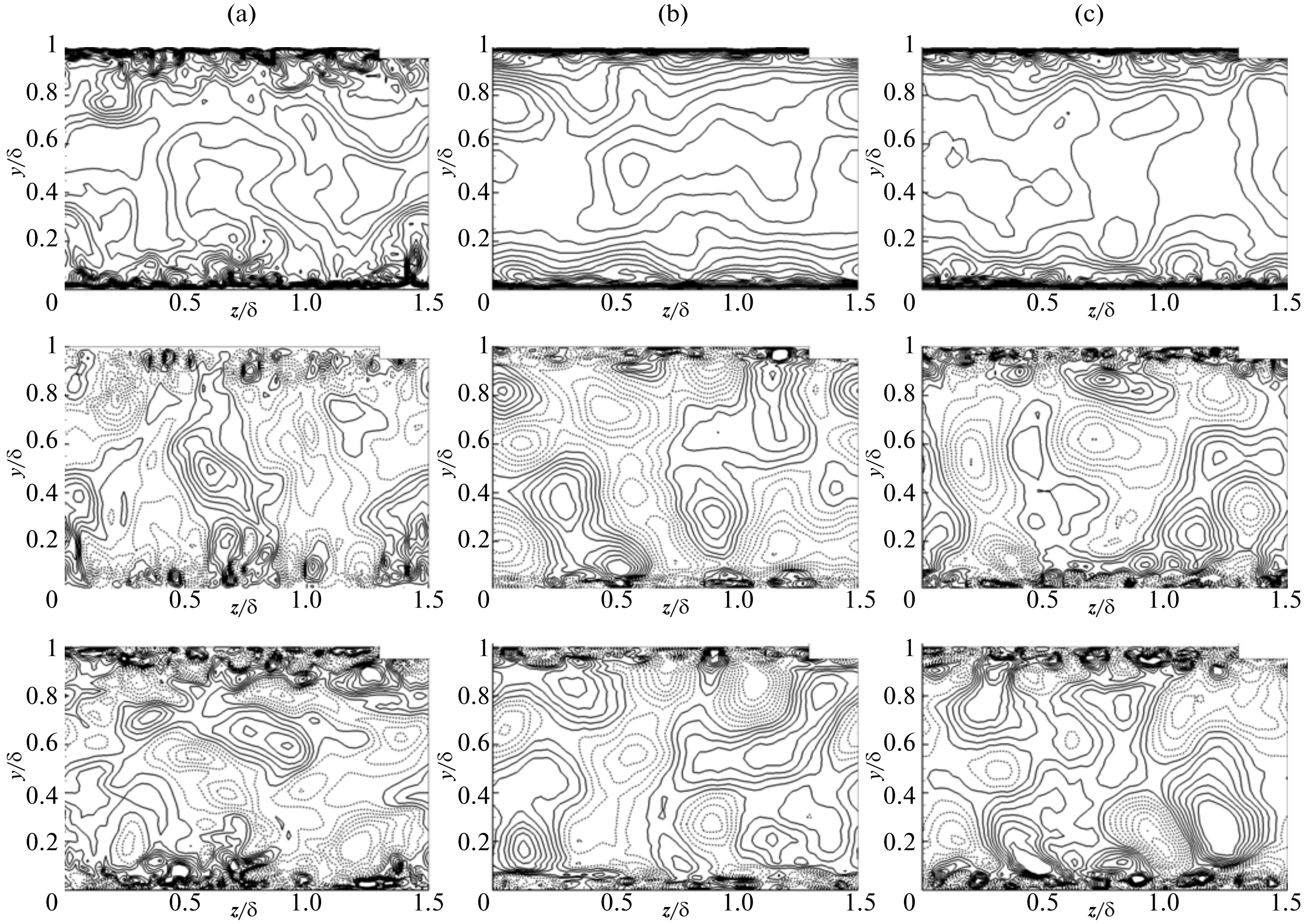

Fig. 4. Comparison of the instantaneous fields of velocity components in the inflow plane for (a) the "reference" calculation and calculations using the (b) initial and (c) modified SEM methods: (*1*) u, (*2*) v, and (*3*) w.

profiles, and then gradually approach them; at $x = 6\delta$, both solutions become almost completely identical.

As for the shear stress profiles also shown in Figs. 1 and 2, the differences between these profiles calculated using the SEM and reference profiles remains rather significant throughout the calculated region.

Thus, having set inflow boundary conditions for the LES using the SEM, the intermediate region length for averaged flow characteristics is $(8-10)\delta$; for shear stresses, it is appreciably larger. This conclusion is consistent with the conclusions of the authors of the SEM [2, 3], which confirms the correctness of its implementation in the present study. This also suggests that, despite the noticeable superiority of the SEM over other known synthetic methods, demonstrated in [2], its error remains rather significant. The causes of the insufficiently rapid restoration of the velocity field are obviously associated with the differences between the synthetic velocity field created by the SEM and the "actual" field formed in the inflow section in reference calculations. A comparison of these fields for the plane-channel flow is shown in Figs. 3 and 4.

Analysis of the eddy fields shown in these figures in various flow sections allows the following conclusions to be drawn.

First, when using the SEM, eddy structures near the inflow section ($x/\delta = 0$) are isotropic, whereas, in the reference calculation, they are significantly extended along the flow near the wall (see Fig. 3). This is quite natural, since the velocity fluctuation anisotropy in the SEM almost is not considered.

Second, the eddy structure sizes in the calculation using the SEM substantially exceed the corresponding sizes of the "reference" field structures, and this discrepancy is observed not only near solid walls, but also at a distance from it (see Fig. 4). This synthetic field defect is associated with the determination of the linear scale σ (7), which is based on the integral turbulence scale l_{turb}. For example, in the logarithmic region of the boundary layer, the value of the latter varies in the range $((2-2.5)d_w$ (d_w is the distance to the wall), while the quantity σ which is the radius of eddy structures generated by the SEM should not exceed d_w.

4. PROPOSED SEM MODIFICATION

To eliminate, or at least soften, the above SEM disadvantages, the following modification of this method is proposed in this paper.

First, to exclude the possibility of generating too large (with sizes exceeding the distance to the wall) eddy structures, the additional factor of 0.5 is introduced into the turbulence scale definition,

$$l_{\text{turb}} = 0.5k_t^{3/2}/C_\mu\omega_t.$$

Second, to provide the desirable anisotropy of generated eddy structures, the longitudinal (in the flow direction) size of local fluctuations near the wall should exceed their transverse size; far from the wall, both sizes should be almost identical. The simplest method to achieve this is the introduction of two scales, i.e., transverse σ_y and longitudinal σ_x ones, which are defined as

$$\sigma_y = \max\left(\min\left(0.5\frac{k_t^{3/2}}{C_\mu\omega}, \kappa\delta\right), \Delta\right), \sigma_x = \max(\sigma_y). \quad (4)$$

For the flow in the boundary layer in which the integral scale l_{turb} nonmonotonically varies with distance from the wall (initially increases and then decreases), the transverse scale definition slightly changes: until reaching the l_{turb} maximum point, it is calculated by formula (4), and then it is set to be constant.

The effect of the described SEM modifications on the channel flow eddy structure is illustrated in Figs. 3 and 4. It follows from the figures that these modifications indeed cause generation of more realistic eddies near the walls: they are substantially anisotropic (extended along the main flow) even in the immediate vicinity from the inflow section (Fig. 3). Furthermore, when using the proposed modifications, the field structure of synthetic velocity pulsations in the y–z inflow plane is in appreciably better agreement with the corresponding structure obtained in the reference calculation than when using the initial SEM (Fig. 4).

The indicated quality improvements of the synthetic turbulence generated on the LES inflow boundary naturally lead to a significant improvement in the LES accuracy. This is confirmed by Figs. 5–8, which compare the results of calculations of two flows under consideration obtained using the initial and modified SEM versions. We can see that the proposed modification leads to a significantly smaller deviation of the calculated results from the reference ones and to a decrease in the length of the intermediate region within which these results are “restored” to the reference values.

For example, for the channel flow, the friction coefficient is almost identical to the reference one (see Fig. 5); for the boundary-layer flow, its deviation from the reference calculation decreases from 30% to 10–15% (see Fig. 6).

The average velocity profiles obtained using the modified SEM (Figs. 7 and 8) almost do not differ from the reference ones. An insignificant difference in them is observed only in the section $x/\delta_0 = 1$ for the boundary–layer flow. However, this is explained not so much by disadvantages of the synthetic velocity field in the inflow section as by the difference between the RANS solution using the k–ω SST model and the LES solution at the relatively low Reynolds number under consideration. Finally, the computational accuracy of

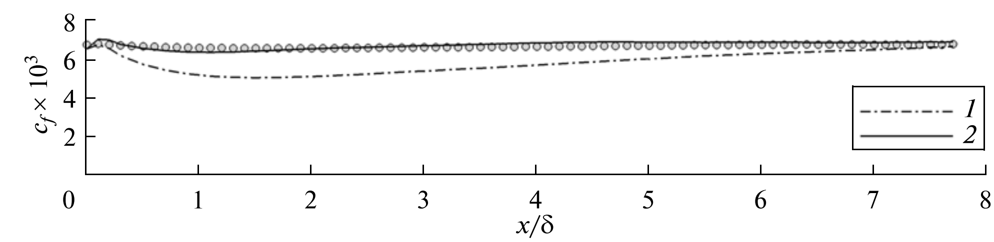

Fig. 5. Distribution of friction coefficient c_f over the longitudinal coordinate for the channel flow: (circles) “reference” calculation, (*1*) original SEM, and (*2*) modified SEM.

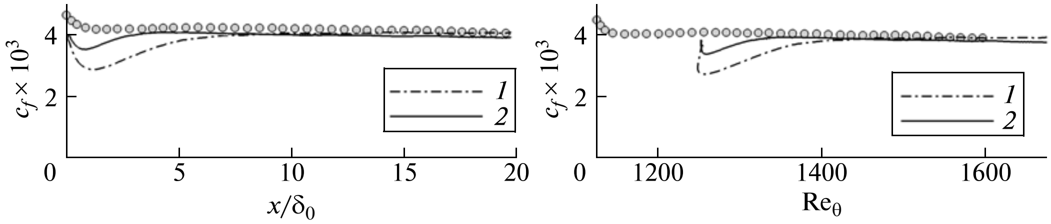

Fig. 6. Distribution of friction coefficient c_f over the longitudinal coordinate and the dependence of the friction coefficient on the Reynolds number Re_θ for the boundary-layer flow: (circles) “reference” calculation, (*1*) original SEM, and (*2*) modified SEM.

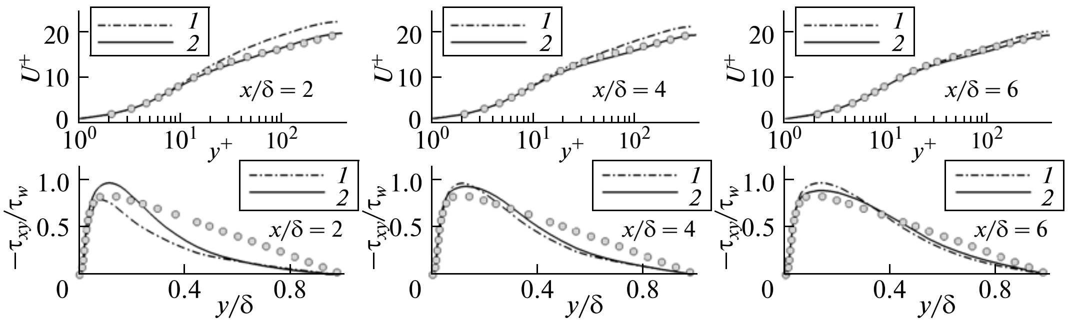

Fig. 7. Development of the average velocity and Reynolds shear stress profiles for the channel flow: (circles) "reference" calculation, (*1*) original SEM, and (*2*) modified SEM.

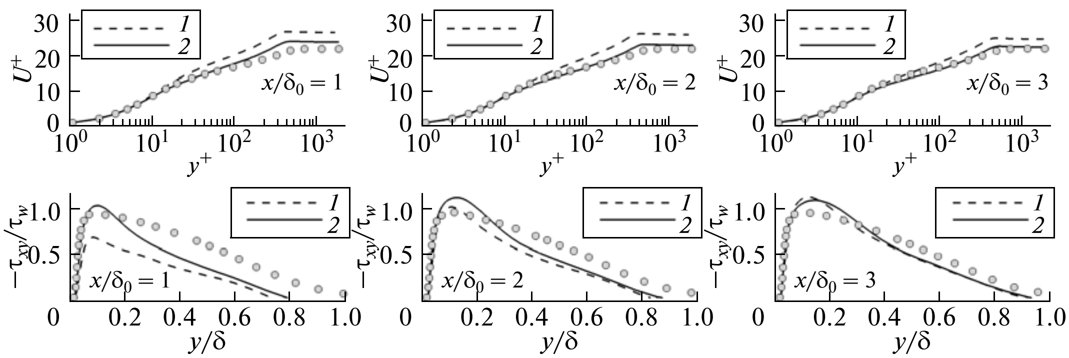

Fig. 8. Development of the average velocity and Reynolds shear stress profiles for the boundary-layer flow: (circles) "reference" calculation, (*1*) original SEM, and (*2*) modified SEM.

the shear stress profiles when using the proposed SEM modification also appreciably increases.

CONCLUSIONS

By means of the example of two canonical turbulent flows (steady plane-channel flow and boundary-layer flat-plate flow), the capabilities of the synthetic eddy method (SEM) developed in [2, 3] were analyzed for setting inflow boundary conditions in calculating turbulent flows using the LES method. Based on this analysis, a modification of the method for determining the linear scale of generated eddy structures, used in the SEM, was proposed. It was shown that, in the calculation of the flows under consideration, this modification makes it possible to significantly decrease the determination error of the averaged flow parameters and to shorten the region in which the transition from synthetic turbulence to the physically realistic field of velocity pulsations occurs.

REFERENCES

1. Sagaut, P., Deck, S., and Terracol, M., *Multiscale and Multiresolution Approaches in Turbulence*, London: Imperial College Press, 2006.
2. Jarrin, N., Benhamadouche, S., Laurence, D., and Prosser, R., *Int. J. Heat Fluid Flow*, 2006, vol. 27, no. 4, p. 585.
3. Jarrin, N., Prosser, R., Uribe, J., Benhamadouche, S., and Laurence, D., *Int. J. Heat Fluid Flow*, 2009, vol. 30, no. 3, p. 435.
4. Batten, P., Goldberg, U., and Chakravarthy, S., *AIAA J.*, 2004, vol. 42, no. 3, p. 485.
5. Van Driest, E.R., *J. Aeronaut. Sci.*, 1956, vol. 23, no. 11, p. 1007.
6. Shur, M., Spalart, P., Strelets, M., and Travin, A., *Int. J. Heat Fluid Flow*, 2008, vol. 29, no. 6, p. 1638.
7. *Notes on Numerical Fluid Mechanics and Multidisciplinary Design*, Garbaruk, A., Magidov, D., Shur, M., Strelets, M., and Travin, A., Eds., Vol. 94: *FLOMANIA—An European Initiative on Flow Physics Modelling: Results of the European-Union Funded Project (2002–2004)*, Berlin: Springer, 2006, p. 101.
8. Rogers, S. and Kwak, D., *Appl. Numer. Math.*, 1991, vol. 8, no. 1, p. 43.
9. Menter, F.R., *AIAA J.*, 1994, vol. 32, p. 1598.
10. Lund, T., Wu, X., and Squires, K., *J. Comput. Phys.*, 1998, vol. 140, no. 2, p. 233.
11. Spalart, P.R., Strelets, M., and Travin, A., *Int. J. Heat Fluid Flow*, 2006, vol. 27, no. 5, p. 902.